RADIATION CLIMATOLOGY OF THE GREENLAND ICE SHEET DERIVED FROM GREENLAND CLIMATE NETWORK DATA

Konrad Steffen, Jason Box
University of Colorado at Boulder
Cooperative Institute for Research in Environmental Sciences
Division of Cryospheric and Polar Processes
Campus Box 216, Boulder CO 80309

NAG5-11612
Final Progress Report
to
National Aeronautics and Space Administration
March 2003

AUTOMATIC WEATHER STATION SADDLE IN SOTUHERN GREENLAND

TABLE OF CONTENTS

1. Analysis of Radiative Fluxes at GC-Net sites, 1996-2001

The magnitude of shortwave and longwave radiative fluxes are critical to surface energy balance variations over the Greenland ice sheet, affecting many aspects of its climate, including melt rates, the nature of low-level temperature inversions, the katabatic wind regime and buoyant stability of the atmosphere. Nevertheless, reliable measurements of the radiative fluxes over the ice sheet are few in number, and have been of limited duration and areal distribution (e.g. Ambach, 1960; 1963, Konzelmann et al., 1994, Harding et al., 1995, Van den Broeke, 1996). Hourly GC-Net radiation flux measurements spanning 1995-2001 period have been used to produce a monthly dataset of surface radiation balance components. The measurements are distributed widely across Greenland and incorporate multiple sensors (Figure 1). The results of this study have been submitted for publication in *The Journal of Applied Meteorology*, March 14, 2003 (Box et al. *submitted*). The study is summarized in the following.

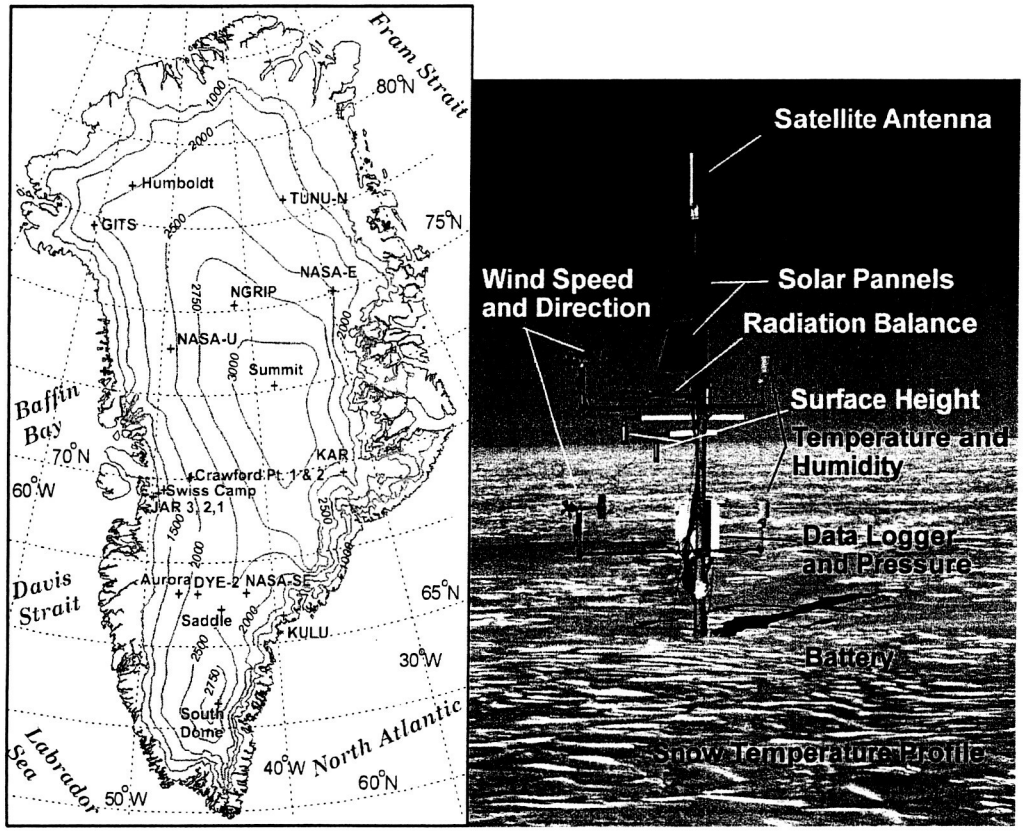

Figure 1. (Left) Greenland map featuring the inland ice region and Greenland Climate Network (GC-Net) locations. (Right) Photo of typical GC-Net Automatic Weather Station

1.1 Surface Radiation Balance

The four components of the surface radiation budget are the incident and reflected short-wave radiation, $S\downarrow$ and $S\uparrow$, respectively, and the incoming and outgoing longwave radiation, $L\downarrow$ and $L\uparrow$, respectively, such that the radiation balance (Q^*) is:

$$Q^* = (S\downarrow - S\uparrow) + (L\downarrow - L\uparrow)$$

Errors and uncertainties in the individual components are identified in comparisons with precise experimental measurements located at 3 diverse GC-Net sites: Swiss Camp; Summit; and Tunu-N.

1.2 Shortwave Radiation

The results of comparisons between operational GC-Net shortwave instruments are summarized in Table 1.

TABLE 1. Daily Average Radiation Fluxes from GC-Net and Calibration Data

Site	Period	Parameter	GC-Net [W m^{-2}]	Experiment [W m^{-2}]	(GC-Net) – (Experiment) [W m^{-2}]	% deviation
Tunu-n	18 May - 30 May, 1996	S↓	351.1	330.4	20.6	6.2
Tunu-n	18 May - 30 May, 1996	S↑	309.2	261.4	47.8	18.3
		Albedo	0.88	0.79	0.09	
Swiss Camp	02 Apr - 23 May, 1999	S↓	209.4	215.2	-5.7	-2.7
Swiss Camp	02 Apr - 23 May, 1999	S↑	185.4	180.8	4.6	2.5
		Albedo	0.89	0.84	0.04	
Summit	30 June - 10 July, 2000	S↓	380.3	387.1	-6.8	-1.8
Summit	30 June - 10 July, 2000	S↑	332.6	309.8	22.8	7.4
		Albedo	0.87	0.80	0.07	

Multi-year monthly average shortwave components for selected representative sites are shown in Figure 2. There is a large annual cycle in down welling shortwave irradiance ($S\downarrow$), from little or no radiation for ~5 months at northern sites in winter to nearly 400 W m^{-2} at the same northern sites and Summit during summer months. Maximum $S\downarrow$ is observed at the high elevation Summit site in June (378 W m^2 5-year June average). Maximum monthly-average $S\downarrow$ measured by the LI-COR sensor in June 2001 was 380 W m^{-2}, while the Kipp and Zonen CM21 sensor measured 396 W m^{-2}. The annual cycle of $S\downarrow$ is less extreme at South Dome, 300 km south of the Arctic Circle and 1800 km south of the northernmost sites. During summer (JJA), $S\uparrow$ values below equilibrium line altitude (ELA) are ~40% lower than over the high elevation sites. The corresponding lower albedo below ELA results in a factor of 3 times as much S^* (155 W m^{-2}) than in the dry snow zone (53 W m^{-2}). S^* increases more rapidly from ELA to the lowest elevations than from the accumulation area to ELA. This is in contrast to modeling results from Van de Wal and Oerlemans (1994), who showed S^* reaching a minimum near the ELA, and slowly increasing again with higher elevations. An elevation increase in $S\downarrow$ is also observed for Iceland's largest icecap and has been attributed to an increase in cloudiness at low elevations (Oerlemans et al., 1999). The amount of water vapor and other background atmospheric absorbers/scatterers also decreases with elevation, resulting in larger $S\downarrow$ values at Summit compared to lower elevations. $S\downarrow$ decreases with elevation at a greater rate

below 1200 m, indicating the importance of greater cloud optical depths at low elevation sites.

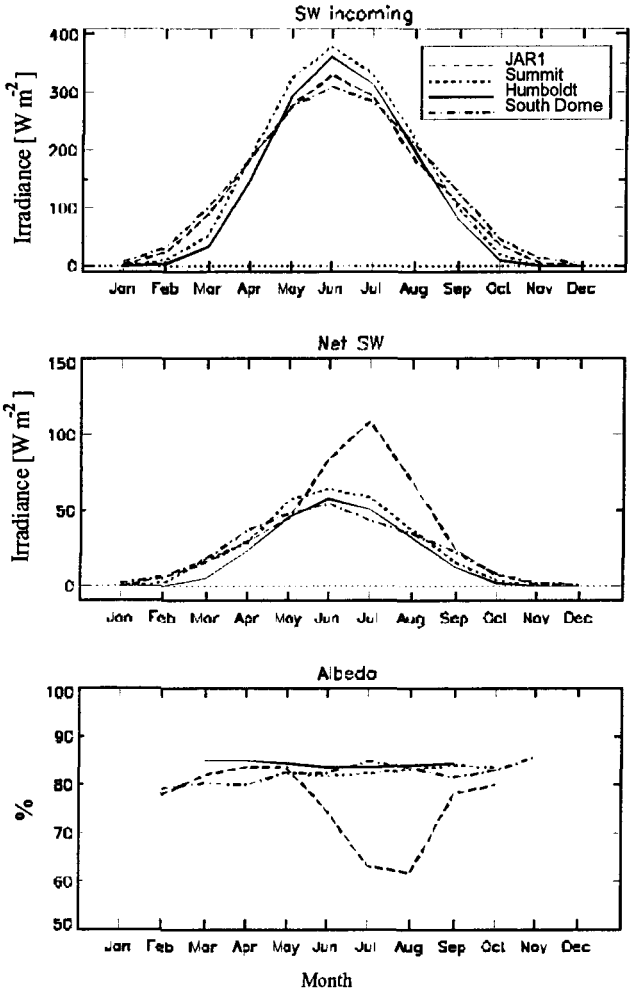

Figure 2. Annual cycle of monthly average down welling and net shortwave irradiance and albedo at selected Greenland Climate Network sites for available data over the 1995-2001 period.

Multi year monthly average absorbed shortwave irradiance *(S*)* reaches values between 50-100 W m^{-2} in summer. There is a large difference in *S** between the dry-snow and ablation zones during the summer months. Peak *S** at low elevation ablation-zone sites in summer is associated with large surface albedo reductions from dry to wet snow, meltwater ponding, and eventually the exposure of melting glacial ice containing significant quantities of dark-grey dust on the surface. A particularly high *S** monthly value of 164 W m^{-2} was observed at JAR1 in July 1996 associated with melt water ponding reaching 1 m depth, as indicated by surface height data. Hourly melt lake minimum albedo was 0.15. The transient melt lake at JAR1 biases the monthly albedo since the melt lake was only present for 8 days in 1996 and 4 days in 1997. Melt lakes cover only a few percent of the

area in that region. The JAR1 AWS has since moved out of the basin where the melt lake forms by 120+ m y^{-1} glacial flow. S^* values exceeding 175 W m^{-2} are observed at the lower elevation JAR2 and JAR 3 sites where there is no evidence of melt lakes in the surface height data. Small ponds have been observed at JAR2 together with large quantities of dust. Minimum monthly average albedo values of 0.42 are observed in the ablation zone at JAR2 and JAR3 in July 2000.

Monthly average S^* reaches maximum values of 70 W m^{-2} at high elevation, dry snow sites, and is commonly ~50 W m^{-2} in summer months at sites above ~1200 m elevation when no melting is occurring. Significant melting does occur at intermediate elevation percolation zone sites, evidenced by above freezing air temperatures, reductions in surface height indicating firn deflation/compaction and minor 0.01 to 0.04 albedo reductions. For example, large intermediate elevation albedo reductions were –0.06 at CP1 in July 1995 and -0.03 at Humboldt in June 1998. There is even a small summertime albedo reduction (-0.01 to –0.02) at the dry snow zone sites of Summit and NGRIP, apparently not caused by above melting temperatures, but by enhanced snow metamorphism, i.e. grain growth, surface depth hoar, given relatively high temperatures and temperature gradients in the near-surface snow layer. The albedo of the dry snow zone remains nearly constant throughout the year with values of 0.84 ±0.05. The all-sky broadband albedo of new snow commonly has a monthly maximum value of 0.88 ±0.02 as measured at Summit with Kipp & Zonen pyranometers

1.3 Shortwave Cloud Radiative Effect

To determine the shortwave cloud radiative effect, measured clear-sky values are compared with hypothetical values calculated from the Arctic-version FluxNet radiative transfer model (Key et al., 1996).

Given that the $S\downarrow$ measurements represent all-sky conditions, the difference between clear sky modeled $S\downarrow$ and measured $S\downarrow$ is the shortwave cloud radiative effect (S_{CRE}). Figure 3 illustrates the difference between modeled clear $S\downarrow$ and the measured downwelling shortwave flux. Monthly average S_{CRE} indicates that, on average, clouds deplete incident solar irradiance. Maximum S_{CRE} amounts are observed at low elevation sites, -150 W m^{-2} in summer months. There is a large difference in July $S\downarrow$ at the low elevation eastern and western sites. At the Kulu AWS site, in the southeast, the July 1999 average $S\downarrow$ is 39% lower than at JAR1, in western Greenland. During this month, S_{CRE} at Kulu was -250 W m^{-2}. The difference in $S\downarrow$ values is due to the much greater cloud optical thickness (i.e. cloud amount) in southeast Greenland as compared to the western part of Greenland (Warren et al. 1986, 1988).

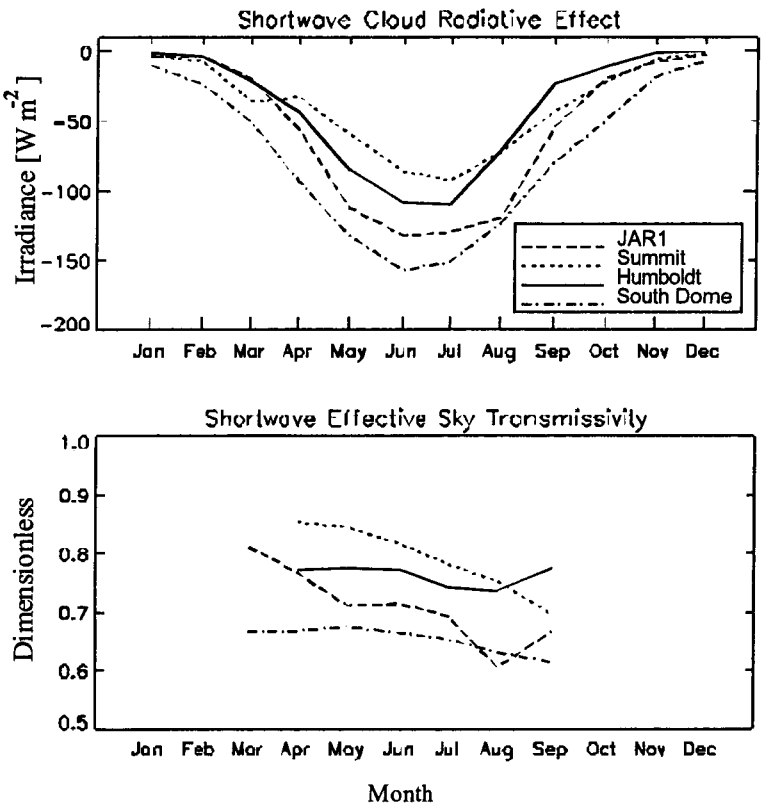

Figure 3. Annual cycle of monthly average shortwave cloud radiative effect and effective sky transmission at selected Greenland Climate Network sites in 1998 and 1999.

Taking the ratio of measured $S\downarrow$ to modeled clear-sky $S\downarrow$ gives a shortwave magnitude-independent measure of effective sky transmissivity (τ_{eff}) (Figure 3). Maximum τ_{eff} values of 0.75-0.85 at Summit indicate the greatest frequency of clear skies or thin clouds among the selected sites. Other sites with relatively high τ_{eff} are NGRIP and Tunu-N. On average, all sites exhibit a spring minimum τ_{eff}. Southern sites exhibit relatively low τ_{eff} (i.e. southern sites are relatively cloudy), e.g. South Dome; Saddle; and particularly, Kulu with July 1999 τ_{eff} value of 0.45. The trends in τ_{eff} observed at most sites are not a leveling error but a trend from relatively clear spring skies to relative cloudy autumn skies, resulting from an increase in cloud amount (Warren et al. 1986, 1988) and water vapor convergence (Serreze et al. 1995) in the later part of the summer.

1.4 Longwave Radiation

Surface emitted longwave irradiance ($L\uparrow$) is calculated using the Stefan-Boltzmann Law of blackbody emission, owing to the fact that snow thermal emmisivity (ε) is very high and nearly constant between 0.985 and 0.990 (Dozier and Warren, 1982).

$$L\uparrow = \varepsilon\sigma T_0^4$$

Parameterized $L\uparrow$ was found to closely approximate precise measurements (Figure 4).

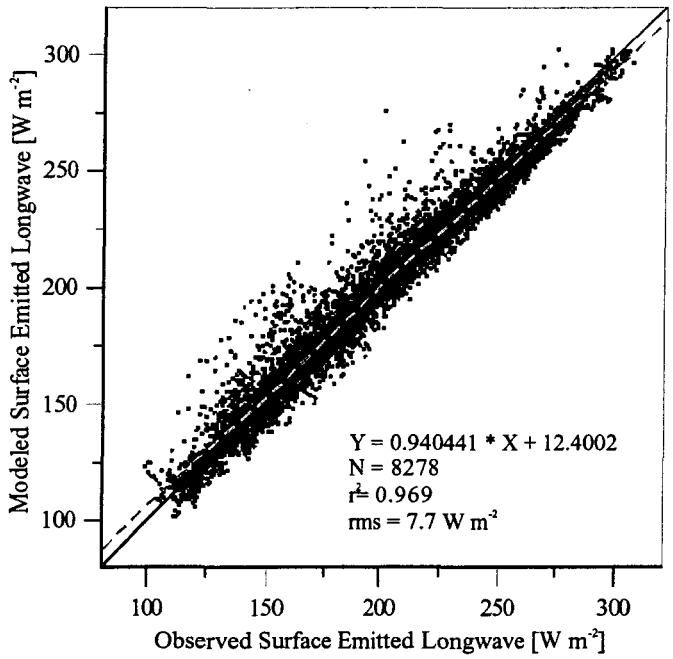

Figure 4. Correlation of 11-months of hourly parameterized surface emitted longwave irradiance with Kipp and Zonen CG4 observations at Summit. The least-squares fit is indicated by a dashed line. The one to one relationship is indicated by a solid line.

A parameterization for down welling longwave radiation $(L\downarrow)$ was derived based on temperature *(T)* and specific humidity *(q)* data in comparison with hourly $L\downarrow$ measured at Summit and Swiss Camp (Figure 5). The two dimensions of this relationship (Figure 5a and 5b) are featured separately to illustrate the clustering of hourly values into classes corresponding roughly to clear, cloudy, mixed, and indistinct conditions. Polynomial coefficients for the quadratic trend surface for the parameterization are given in Table 2.

TABLE 2. Polynomial Coefficients for Down welling Longwave Parameterization

Site	Constant (a0)	T [°C] (a1T)	T [°C] (a2T)	T [°C] q [g kg^{-1}] (Tq)	q [g kg^{-1}] (a1q)	q [g kg^{-1}] (a2q)
Summit	-80.706	-9.024	-0.111	-4.783	58.745	0.19
Swiss Camp	106.953	-0.628	0.001	-3.442	23.138	5.167
Combination	109.075	-2.341	-0.051	-1.453	35.502	1.57

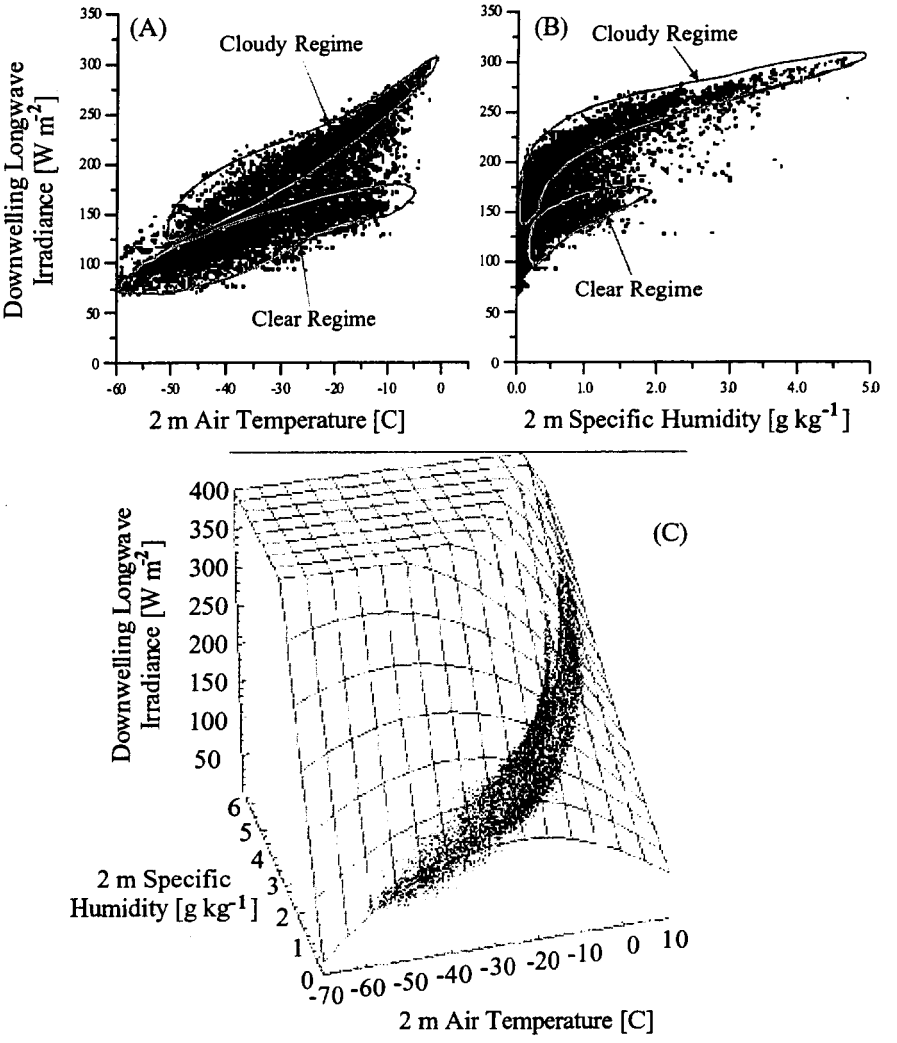

Figure 5. *Correlation of observed Kipp and Zonen CG4 down welling longwave irradiance with 2 m temperature (A) and 2 m specific humidity (B). (C) Illustration of 3-dimensional correlation of 2 m temperature and 2 m specific humidity with the observed down welling longwave irradiance from 13000 cases equally divided between Swiss Camp and Summit observations.*

Multi-year average monthly longwave components for selected sites are given in Figure 6. Parameterized down welling longwave irradiance *(L↓)* exhibits an annual cycle, peaking in August or July, with minimum in February and March. In June and July $L\downarrow$ fluxes are nearly equivalent among the sites, ranging from 230-255 W m^{-2}. In August, JAR1 and South Dome values increase to a maximum of 260 W m^{-2}. $L\downarrow$ at high elevations or high latitudes such as Summit or Humbloldt have a similar annual cycle but ~50 W m^{-2} lower in magnitude, mainly during the winter months. High elevation and northern winters exhibit a constant minimum value, indicative of relatively cloudless conditions, while low elevation and southern stations exhibit a more distinct spring minimum. Monthly summer averages of $L\downarrow$ are predominantly smaller than surface emitted longwave irradiance *(L↑)*, resulting in a continual loss of thermal radiant energy by the ice sheet surface. Outgoing longwave irradiance *(L↑)* is a function of surface air temperature, peak-

ing in summer with magnitudes between 250 W m^{-2} and 316 W m^{-2}. A melting surface with 0° C temperature has an irradiance value close to 316 W m^{-2}. The amplitude of the annual cycle is between 110 W m^{-2} and 130 W m^{-2}. This coreless winter is often followed by an abrupt $L\uparrow$ increase normally between March and May, corresponding with the abrupt spring temperature rise that is accompanied by a 16-22 hPa pressure rise (Rogers et al. 1997).

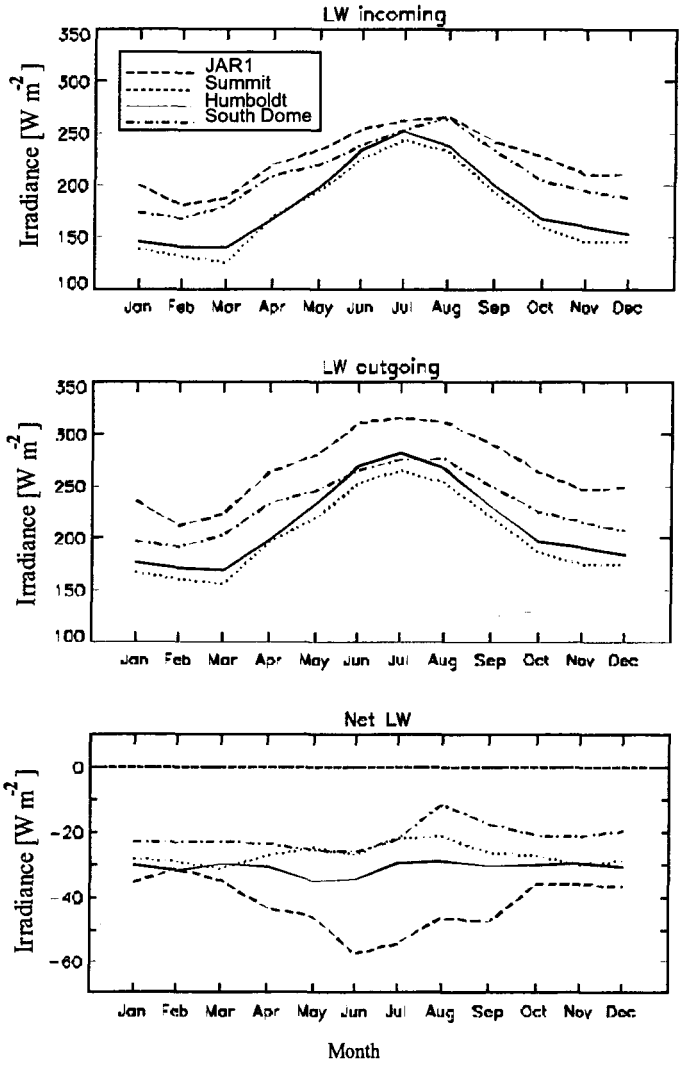

Figure 6. Annual cycle of monthly average down welling, outgoing, and net longwave irradiance at selected Greenland Climate Network sites for available data over the 1995-2001 period.

Net longwave irradiance *(L*)* is consistently negative throughout the year. Still, relative shifts in L^* magnitude influence summertime surface heating and melt rates. At southern and southeastern sites, L^* approaches positive values in late summer. This is indicative of $L\downarrow$ dominating the longwave radiation balance, apparently due to relatively warm clouds. Winter L^* values are between –15 W m^{-2} and –35 W m^{-2}. Summit and JAR1 have similar L^* magnitudes throughout the year despite 50 W m^{-2} smaller values in down welling and emitted longwave fluxes at Summit.

The importance of net longwave radiation for surface heating and melt processes is more apparent in terms of year to year variability.

1.5 Net Radiation

Net radiation *(Q*)*, based on measured incoming and reflected shortwave and modeled net longwave, is positive in summer at all sites (Figure 7). Maximum Q^* values occur in June and July at low elevation sites (e.g. JAR1). At low elevation sites in summer, Q^* is dominated by a reduction in surface albedo and high values of down welling shortwave radiation. S^* dominates melt potential in summer given that L^* exhibits maximum negative values in summer. The magnitudes of monthly averages of S^* are always greater than the L^* magnitudes in summer. Still, L^* interannual variability is of importance in adjusting surface melt, in particular $L\downarrow$. Peak Q^* values at dry snow sites are between 5 W m^{-2} and 25 W m^{-2} in summer, as also described by Cullen and Steffen (2001). In winter, $L\uparrow$ dominates the radiation balance, despite the common temperature inversion. Peak negative Q^* values occur in winter at low elevation sites, e.g. -30 W m^{-2} at JAR1. An extremely high value at JAR1 in July 1996 (110 W m^{-2}) was caused by the development of a 1 m deep melt lake flooding the site. South Dome modeled Q^* values are positive on average for the months March through September and less negative for the remaining part of the year. throughout the year. These estimates are perhaps not well represented by the combined Summit-Swiss Camp $L\downarrow$ parameterization and therefore in error given the different climate regime at South Dome. A similar bias may exist for sites in the far north that is not reconciled here, owing to the lack of validation data at these remote sites. Net radiation accuracy of ±14 W m^{-2} as derived from monthly comparisons with Summit data, represents the combined errors in 4 radiation components.

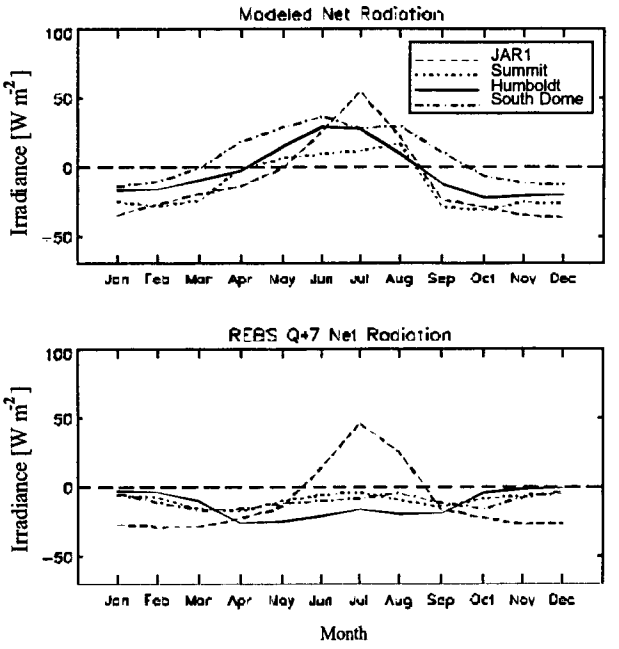

Figure 7, Annual cycle of monthly average net radiation at selected Greenland Climate Network sites for available data over the 1995-2001 period.

1.6 Interannual Variability

The interannual range of radiation fluxes at two different sites, JAR1, in the ablation zone,

and Summit, in the dry snow zone, are shown in Figure 8. The range is the absolute value of the difference between values at a given site over 1996-2001. All parameters but temperature exhibit a summer interannual variability maximum. Low elevation (JAR1) variability seems to be dominated by shortwave fluxes, while the longwave fluxes appear to dominate the high elevation variability, owing to the fewer or thinner high elevation clouds and nearly constant surface albedo. Down welling shortwave flux ($S\downarrow$) varies more interannually at low elevations sites (60 W m^{-2}) than at sites above 1200 m due to the fact that there is a greater frequency of relatively thick clouds below 1000 m elevation on the ice sheet, having their origin over nearby coastal waters. Albedo variability is the single most influential parameter to the surface radiation balance variability at low elevation sites. $S\uparrow$ variability is ~20% larger than $S\downarrow$ variability. S^* variability is a factor of 2 larger than L^* variability. At low elevation sites, L^* variability is greatest in summer, again indicating the important influence of clouds. Interannual variability of $L\downarrow$ (40-80 W m^{-2}) peaks in summer months. L^* variability is smaller (10–20 W m^{-2}) in magnitude than net shortwave radiation variability, particularly at ablation zone sites. These observations appear to differ from Ohmura (2001) but closer inspection of the method he adopts to partition energy sources versus sinks explains this dissimilarity. Rather than comparing L^* versus S^* as sources of melt for radiation, Ohmura (2001) characterizes $L\downarrow$ as an independent source, which is a larger term than the absorbed global radiation.

There are numerous cases of interannual variability of radiation components at different GC-Net sites that are controlled by changes in temperature, humidity, melt rates and cloudiness. To illustrate this, a comparison is made between springtime in the relatively warm 1998 and the cold 1999. In 1998, humidity was relatively high, while in 1999 humidity was low. Surface height reductions at JAR1 between April and August in 1998 (-1.9 m) are 30% greater than in 1999 (-1.3 m). JAR1's annual surface height change is –1.16 m in 1998 and -0.15 m in 1999. Figure 9 shows that opposing trends in the radiation components are observed, between the two years.

$S\downarrow$ anomalies are negative in spring 1998, consistent with greater than normal values of humidity and temperature, which results in a large $L\downarrow$ that implies greater than normal cloud amount. The temperature and/or low accumulation led to lower than normal albedo in 1998 and much higher albedo in May and June 1999. June 1999 was apparently both relatively cold and clear. August 1999 has high net radiation values owing to low surface albedo, caused by melt of the relatively thin snow pack, and because there was no superimposed ice remaining after the 1998 melt season. Between 22 May – 27 May, 1998, Nipher gauge measurements totaled 6.6 cm of mixed rain and snow at Swiss Camp. An early onset of melt in western Greenland in 1998 was observed to be triggered by this rainfall. This early melt onset contributed to a 29 cm ice loss at the equilibrium line altitude owing to the earlier than normal loss of seasonal snow, and importantly resulted in early exposure of low albedo glacier ice to peak insolation later in July and August. Not surprisingly, the L^* anomalies are relatively small in magnitude as compared to the S^* anomalies. Similarly, there is a poor relationship between net radiation and the temperature anomalies, consistent with the results of Ohmura (2001). The main difference in these two cases is that the 1999 net radiation is much more negative in June, when the majority of surface melting, under peak annual insolation, typically occurs. The summer 1999 negative net radiation anomaly case is linked with a negative anomaly in $S\downarrow$ and a positive anomaly in $S\uparrow$. In 1998, L^* values are less negative than in other years, implying the dominance of $L\downarrow$ over $L\uparrow$,

despite that L^* still represents a loss of energy from the surface over monthly and longer time scales.

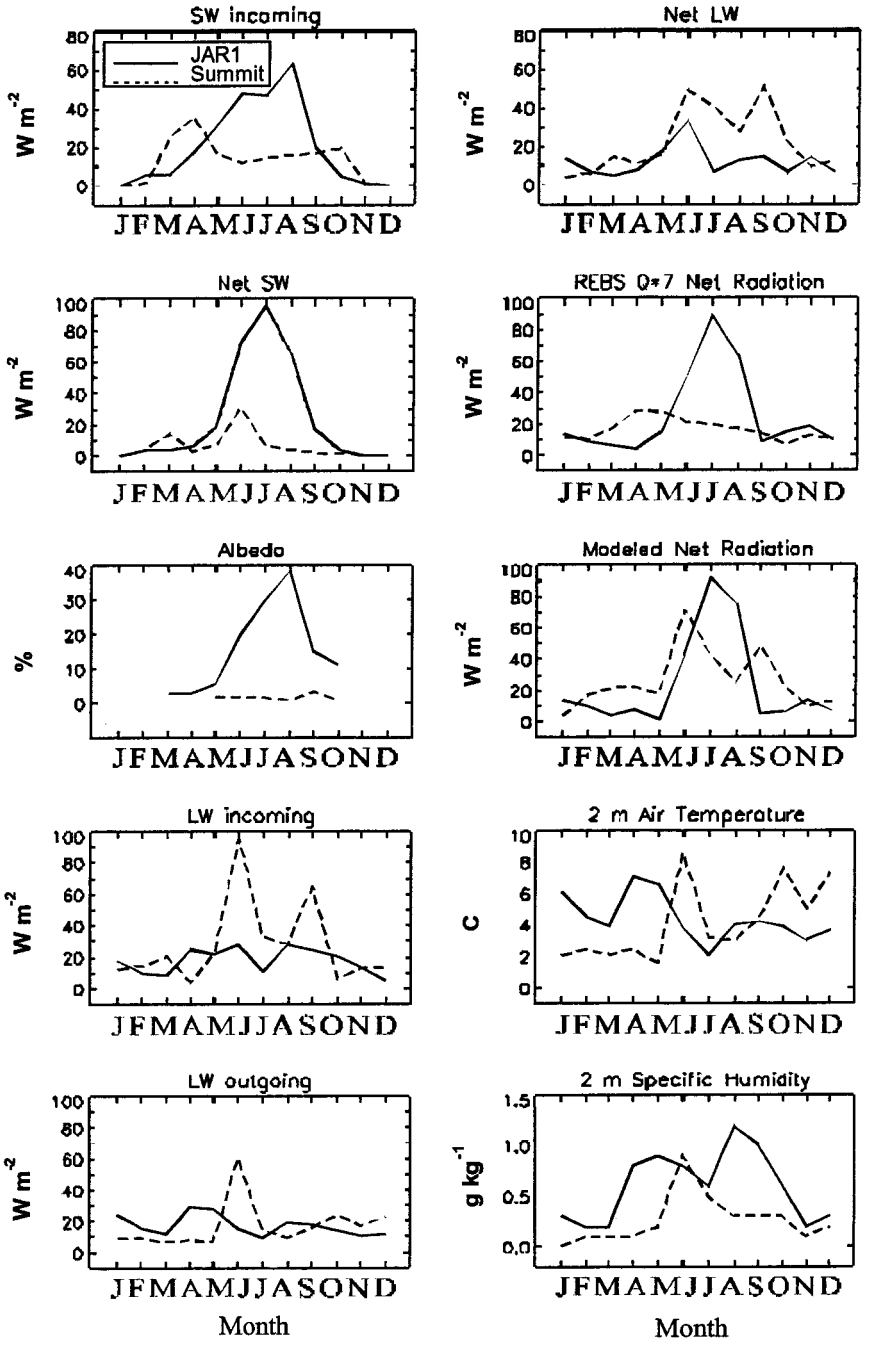

Figure 8, Annual cycle of interannual range in monthly average shortwave and longwave fluxes at JAR1 (solid line) and Summit (dashed line) for data over the 1996-2001 period.

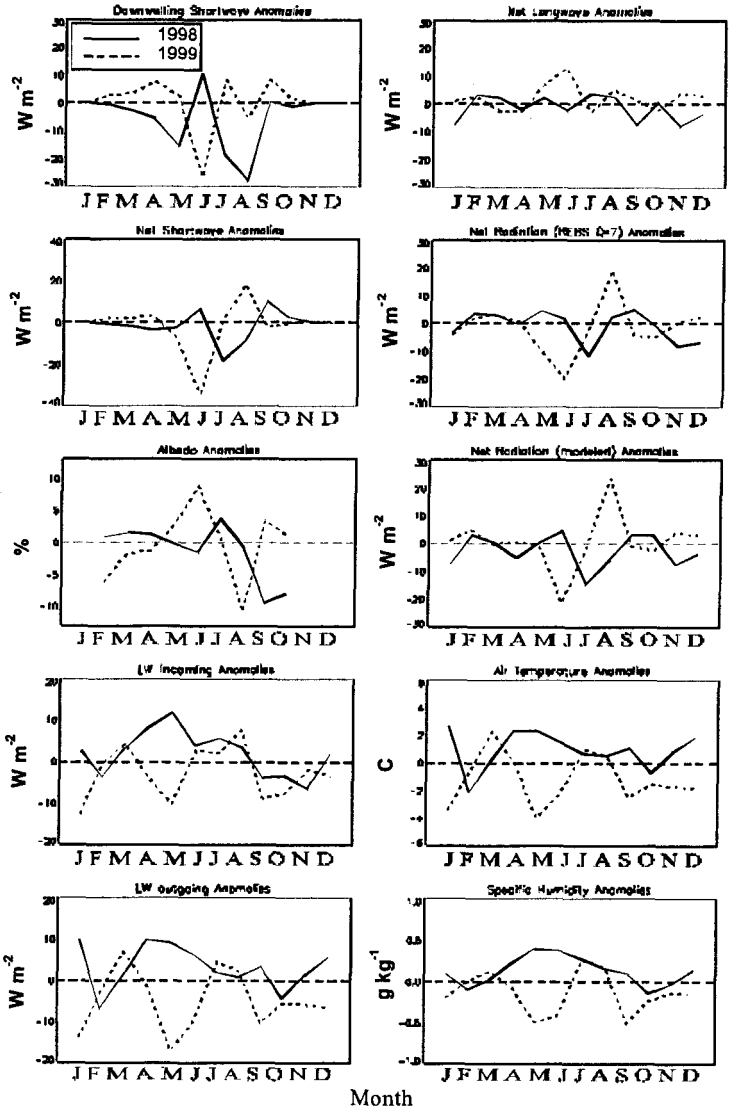

Figure 9, Annual cycle of monthly average anomalies (over 1996-2001) at the JAR1 sites in 1998 and 1999.

$S\downarrow$ anomalies are negative in spring 1998, consistent with greater than normal values of humidity and temperature, which results in a large $L\downarrow$ that implies greater than normal cloud amount. The temperature and/or low accumulation led to lower than normal albedo in 1998 and much higher albedo in May and June 1999. June 1999 was apparently both relatively cold and clear. August 1999 has high net radiation values owing to low surface albedo, caused by melt of the relatively thin snow pack, and because there was no superimposed ice remaining after the 1998 melt season. Between 22 May – 27 May, 1998, Nipher gauge measurements totaled 6.6 cm of mixed rain and snow at Swiss Camp. An early onset of melt in western Greenland in 1998 was observed to be triggered by this rainfall. This early melt onset contributed to a 29 cm ice loss at the equilibrium line altitude owing to the earlier than normal loss of seasonal snow, and importantly resulted in early exposure of low albedo glacier ice to peak insolation later in July and August.

Not surprisingly, the L^* anomalies are relatively small in magnitude as compared to the S^* anomalies. Similarly, there is a poor relationship between net radiation and the temperature anomalies, consistent with the results of Ohmura (2001). The main difference in these two cases is that the 1999 net radiation is much more negative in June, when the majority of surface melting, under peak annual insolation, typically occurs. The summer 1999 negative net radiation anomaly case is linked with a negative anomaly in $S\downarrow$ and a positive anomaly in $S\uparrow$. In 1998, L^* values are less negative than in other years, implying the dominance of $L\downarrow$ over $L\uparrow$, despite that L^* still represents a loss of energy from the surface over monthly and longer time scales.

1.7 Discussion of Errors and Uncertainty

GC-Net shortwave radiation fluxes were compared with measurements made with Eppley PSP instruments at Swiss Camp and Tunu-N. Comparative measurements were also available from an experiment at Summit, where shortwave irradiance was measured at 1.3 - 1.8 m above the snow surface with Kipp and Zonen CM21 pyranometers. The CM21 instruments were heated and ventilated using the Kipp and Zonen CV2 instrument housing. Comparison of incoming shortwave irradiance from LI-COR pyranometers (used at GC-Net sites), Kipp and Zonen (CM21), and Eppley (PSP) pyranometers show good agreement (Table 3). Negative 200SZ biases occurred under clear-skies with solar zenith angles (SZA) exceeding 80°. Because solar irradiance values are small when SZAs are large they have little impact on the surface energy balance. During cloudy conditions, the accuracy of 200SZ measurements is maintained, even for large SZAs since diffuse radiation is dominant.

There are 3 common data errors at all sites that include, firstly, levelling problems of the LI-COR pyranometers. The GC-Net towers have been anchored with steel cables to withstand strong katabatic winds, but because of firn differential compaction, tower and instrument levels have been observed to drift. Pyranometers are levelled during site visits (1-2 years apart) but levelling errors have still been found to be less than 2° for all but extreme cases. While levelling errors have not been corrected, analysing monthly averages reduces this effect. Further, the use of steel cables has been abandoned in recent years, given the recurring instrument level-drift. Secondly, persistent frost on shortwave sensors has led to spuriously low incoming shortwave radiation data at several GC-Net sites (e.g. early spring of 1998 at Tunu-N, NGRIP, and Humboldt). Hence, monthly average data for March 1998 are omitted from this analysis at these sites. NASA-E data are omitted for the same reason during March and April 1998. Thirdly, negative biases in shortwave irradiance have also occurred when instrument towers have shaded radiometers or snow surfaces during periods of low sun angles from the north. The radiative fluxes derived from photoelectric diode and pyranometer thermopile measurements are summarized in Table 3 as daily averages.

Reflected shortwave radiation values required an offset, 6.6% on average for albedo, to compensate for a positive bias caused by the limited spectral sensitivity of the LI-COR 200SZ pyranometer over snow. Down welling shortwave radiation measured by the LI-COR instrument compared within a few % with the Eppley PSP and Kipp and Zonen CM21 measurements. Surface emitted longwave irradiance was derived using a blackbody approximation and extrapolation of the observed temperature profile to estimate surface skin temperature. Down welling longwave radiation was parameterized using 2 m observations of air temperature and

specific humidity. Monthly rms errors of this parameterization are between 11 W m^{-2} and 14 W m^{-2} at the intercomparison sites. Measured down welling and reflected shortwave radiation combined with parameterized longwave fluxes produced more realistic annual cycles of net radiation than those directly measured by the unventilated REBS Q*7 instrument, owing to the instrument's susceptibility to dome interior rime frost development. Largest REBS errors were observed at high elevation sites, particularly in winter. The domeless Kipp and Zonen NR-Lite results did not compare favorably either with our modeled net radiation values or the data from the precise 4-component derived net radiation Modeled net radiation compared well at low elevation sites with REBS data, given that the REBS instrument is though to perform reasonably well at low elevation sites, where air temperatures are sufficiently high to allow desiccants to keep instrument domes dry, and wind speeds are highest.

1.8 Conclusions

In-situ measurements from a network of 20 Greenland ice sheet automated weather stations (GC-Net) were used to produce a set of monthly average shortwave and longwave irradiance components. The largest magnitude and variability of radiation exchanges have been observed at low elevation sites. Low elevation variability is linked to changes in melt and cloud conditions. Rain was observed to initiate early onset of melt at the equilibrium line altitude in western Greenland in 1998 with a below average winter snow cover. Temperature and surface albedo are key parameters in low elevation radiation balance variability. Monthly net longwave irradiance modulates melt, despite representing a continual loss of energy from the surface. This is true given that down welling longwave variability during the melt season is larger than outgoing longwave radiation. At the lower elevations, where substantial seasonal melting occurs, net shortwave radiation fluxes (and their variability) are greater in magnitude than net longwave fluxes. This implies that both albedo and cloud variability are critical in determining the influence of radiation on ablation zone melt intensity.

1.9 Future Work

This work has laid the foundation for future investigations using GC-Net radiation data, now that the monthly variations in radiation parameters have been evaluated climatologically. Numerous process and validation studies may be supported by GC-Net radiation data. We would gain additional insight to investigate hourly data in more detail.

REFERENCES

Ambach, W., Investigations of the heat balance in the area of ablation on the Greenland ice cap, preliminary communication, Archiv für Meteorologie, Geophysik und Boklimatologie, Ser. 13, Band 10, Heft 3, 279-288, 1960.

Ambach, W., Untersuchungen zum Energieumsatz in der Ablationszone des gronlandischen Inlandeises (Camp IV-EGIG, 69° 40'05 N, 49° 37'58 W). Medd. Gronl., 174, 4, 1963.

Box , J. E., N. J. Cullen, K. Steffen, Greenland Ice Sheet Surface Radiative Fluxes, submitted to *Journal of Applied Meteorology*, March 14, 2003

Cullen, N.J., and Steffen, K. Unstable near-surface boundary layer conditions in summer on top of the Greenland ice sheet, Geophys. Res. Lett., 28, 4491-4493, 2001.

Dozier, J., and Warren, S. G., Effect of viewing angle on the infrared brightness temperature of snow, Water Resources Research, 18,.1424-1434, 1982.

Harding, R.J., R.C. Johnson, and H. Soegaard, The energy balance of snow and partially covered areas in western Greenland, Int. J. Climatol., 15, 1043-1058, 1995.

Key, J. R., E. Amano, and J. Collins, *FluxNet User's Guide*, Version 1.0 beta, Technical Report 96-03, Department of Geography, Boston University, 18 pp, 1996.

Konzelmann, T., R. S. W. van de Wal, W. Greuell, R. Bintanja, E. A. C. Henneken, and A. Abe-Ouchi, Parameterization of global and longwave incoming radiation for the Greenland ice sheet, Glob. Planet. Change, 9(1/2), 143-164, 1994.

Oerlemans, J., Bjornsson, H., Kuhn, M., Obleitner, F., Palsson, F., Smeets, C. J. P. P., Vugts, H. F. and de-Wolde, J., Glacio-meteorological studies on Vatnajokull, Iceland: an overview, Boundary Layer Met., 92(1), 3-26, 1999.

Ohmura, A., Physical basis for the temperature-based melt-index method, J. Appl. Met., 40, 753-761, 2001.

Rogers, J. C., R. A. Hellstrom, E. Mosley-Thompson, C-C. Wang, An abrupt spring temperature rise over the Greenland ice cap, J. Geophys. Res., 102(D12), 13793-13800, 1997.

Steffen, K. and J. E. Box, Surface climatology of the Greenland ice sheet: Greenland Climate Network 1995-1999, J. Geophys. Res., 106(D24), 33951-33964, 2001.

Van de Wal, R.S.W., and Oerlemans, J., An energy balance model for the Greenland ice sheet. *Global and Planetary Change*, **9**, 115-131, 1994.

Van den Broeke, M. R., Characteristics of the lower ablation zone of the west Greenland ice sheet for energy-balance modelling, Ann. Glaciol. 23, 160-166, 1996.

Warren, S. G., C. J. Hahn, J. London, R. M. Chervin, R. Jenne, 1986: Global distribution of total cloud cover and cloud type amounts over land, NCAR Tech. Note, Tn-273 +STR, Boulder, CO. 29pp.

Warren, S. G., C. J. Hahn, J. London, R. M. Chervin, R. Jenne, 1988: Global distribution of total cloud cover and cloud type amounts over the ocean, NCAR Tech. Note, Tn-317 +STR, Boulder, CO, 41pp.

APPENDIX

Beginning in 1995, automatic weather stations have been installed on the Greenland ice sheet as part of NASA's Program for Arctic Regional Climate Assessment (PARCA) (Figure 1). Between 1 and 5 stations have been added to the network each year since 1995. As of mid 2001, the Greenland Climate Network (GC-Net) consisted of 20 stations distributed widely over Greenland's inland ice. The system samples 27 surface climate parameters over 15 second to 10 minute time-scales (Table 2), and averages, stores and transmits the hourly data via GOES and ARGOS communication satellites. The hourly data have been quality checked by visual inspection and filtered using statistical methods (Steffen and Box, 2001).

TABLE 1. Greenland Climate Network site information

Station	N-Latitude and W-Longitude	Elevation (m)	Installation Date
ETH/CU Swiss Camp	69° 34' 06", 49° 18' 57"	1149	1995.38
CP1	69° 52' 47", 46° 59' 12"	2022	1995.39
NASA-U	73° 50' 31", 49°, 29' 54"	2369	1995.41
GITS	77° 08' 16", 61° 02' 28"	1887	1995.43
Humboldt	78° 31' 36", 56° 49' 50"	1995	1995.47
Summit	72° 34' 47", 38° 30' 16"	3254	1996.37
Tunu-N	78° 01' 00", 33° 59' 38"	2113	1996.38
DYE-2	66° 28' 48", 46° 16' 44"	2165	1996.40
JAR1	69° 29' 54", 49° 40' 54"	962	1996.47
Saddle	66° 00' 02", 44° 30' 05"	2559	1997.30
South Dome	63° 08' 56", 44° 49' 00"	2922	1997.31
NASA-E	75° 00' 00", 29° 59' 59"	2631	1997.34
CP2	69° 54' 48", 46° 51' 17"	1990	1997.36
NGRIP	75° 05' 59", 42° 19' 57"	2950	1997.52
NASA-SE	66° 28' 52", 42° 19' 20"	2425	1998.31
KAR	69° 41' 58", 32° 59' 59"	2400	1999.37
JAR2	69° 25' 12", 50° 03' 27"	568	1999.42
KULU	65° 45' 35", 39° 36' 12"	878	1999.47
JAR3	69° 23' 44", 50° 18' 37"	323	1999.41
Aurora	67° 08' 06", 47° 16' 28"	1798	2000.48

TABLE 2. GC-Net Instruments Employed in this Study

Location	Parameter/	Instrument	Spectral Sensitivity [μm]	Approximate Uncertainty	Sampling Rate
GC-Net Sites	Down welling Shortwave	LI-COR 200SZ	0.4 - 1.1	5%	
	Upwelling Shortwave	LI-COR 200SZ	0.4 - 1.1	10%	
	Net Radiation	REBS Q*7	0.35 – 30	20%	15 s
	Air Temperature	Vaisala 50YC		0.1 °C	60 s
	Air Temperature	Type-E Thermocouple		0.1 °C.	15 s
	Relative humidity	Vaisala INTERCAP or Vaisala HUMICAP 180		5% < 90% RH 3% > 90% RH	60 s
	Surface height change	Campbell Sci. SR-50		1 mm	10 min
	Multiplexer	Campbell Sci. AM-25T		-	-
	Data logger	Campbell Sci. CR-10/10X		-	-
Summit	Down welling Shortwave	Kipp and Zonen CM 21 Pyranometer	0.305 - 2.800	2%	1 s
	Upwelling Shortwave	Kipp and Zonen CM 21 Pyranometer	0.305 - 2.800	2%	1 s
	Down welling Longwave	Kipp and Zonen CG4 Pyrgeometer	4.5 – 42	4%	1 s
	Upwelling Longwave	Kipp and Zonen CG4 Pyrgeometer	4.5 – 42	4%	1 s
	Net Radiation	combination of above 4 components		5%	1 s
Swiss Camp	Down welling Shortwave	Eppley Pyranometer	0.2 - 3.5	7%	1 s
	Upwelling Shortwave	Eppley Pyranometer	0.2 - 3.5	7%	1 s
	Down welling Longwave	Eppley Pyrgeometer	4 - 50	15%	15 s
Tunu-N	Down welling Shortwave	Eppley Pyranometer	0.2 - 3.5	7%	1 s
	Upwelling Shortwave	Eppley Pyranometer	0.2 - 3.5	7%	1 s